NASA TECHNICAL NOTE

NASA TN D-8492

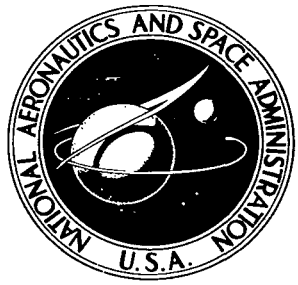

COMPUTER PROGRAM FOR ANALYSIS OF COUPLED-CAVITY TRAVELING-WAVE TUBES

Denis J. Connolly and Thomas A. O'Malley

Lewis Research Center
Cleveland, Ohio 44135

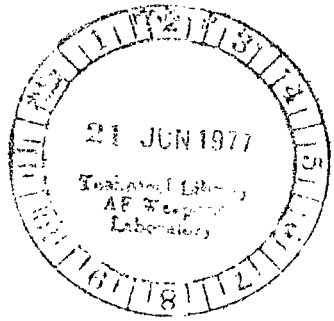

NATIONAL AERONAUTICS AND SPACE ADMINISTRATION • WASHINGTON, D. C. • MAY 1977

1. Report No. NASA TN D-8492	2. Government Accession No.	3. Recipient's Catalog No.
4. Title and Subtitle COMPUTER PROGRAM FOR ANALYSIS OF COUPLED-CAVITY TRAVELING-WAVE TUBES		5. Report Date May 1977 6. Performing Organization Code
7. Author(s) Denis J. Connolly and Thomas A. O'Malley		8. Performing Organization Report No. E-8839 10. Work Unit No. 506-20
9. Performing Organization Name and Address National Aeronautics and Space Administration Lewis Research Center Cleveland, Ohio 44135		11. Contract or Grant No. 13. Type of Report and Period Covered Technical Note
12. Sponsoring Agency Name and Address National Aeronautics and Space Administration Washington, D.C. 20546		14. Sponsoring Agency Code

15. Supplementary Notes

16. Abstract

A flexible, accurate, large-signal computer program has been developed for the design of coupled-cavity traveling-wave tubes. The program is written in FORTRAN IV for an IBM 360/67 time-sharing system. The beam is described by a disk model, and the slow-wave structure by a sequence of cavities, or cells. The computational approach is arranged so that each cavity may have geometrical or electrical parameters different from those of its neighbors. This allows the program user to simulate a tube of almost arbitrary complexity. Input and output couplers, severs, complicated velocity tapers, and other features peculiar to one or a few cavities may be modeled by a correct choice of input data. The beam-wave interaction is handled by a new approach in which the radio-frequency fields are expanded in solutions to the transverse magnetic wave equation. All significant space harmonics are retained. The program was used to perform a design study of the traveling-wave tube developed for the Communications Technology Satellite. Good agreement was obtained between the predictions of the program and the measured performance of the flight tube.

17. Key Words (Suggested by Author(s))	18. Distribution Statement
Coupled-cavity traveling-wave tubes Computer analysis One-dimensional analysis Large-signal analysis	Unclassified - unlimited STAR Category 32

19. Security Classif. (of this report)	20. Security Classif. (of this page)	21. No. of Pages	22. Price*
Unclassified	Unclassified	52	A04

* For sale by the National Technical Information Service, Springfield, Virginia 22161

CONTENTS

COMPUTER PROGRAM FOR ANALYSIS OF COUPLED-CAVITY TRAVELING-WAVE TUBES

by Denis J. Connolly and Thomas A. O'Malley

Lewis Research Center

SUMMARY

A flexible, accurate, large-signal computer program has been developed for the design of coupled-cavity traveling-wave tubes. The program is written in FORTRAN IV for an IBM 360/67 time-sharing system. The beam is described by a disk model, and the slow-wave structure by a sequence of cavities, or cells. The computational approach is arranged so that each cavity may have geometrical or electrical parameters different from those of its neighbors. This allows the program user to simulate a tube of almost arbitrary complexity. Input and output couplers, severs, complicated velocity tapers, and other features peculiar to one or a few cavities may be modeled by a correct choice of input data. The beam-wave interaction is handled by a new approach in which the radio-frequency fields are expanded in solutions to the transverse magnetic wave equation. All significant space harmonics are retained. The program was used to perform a design study of the traveling-wave tube developed for the Communications Technology Satellite. Good agreement was obtained between the predictions of the program and the measured performance of the flight tube.

INTRODUCTION

Numerous works describing large-signal computer programs for traveling-wave tubes have appeared in the past 20 years. A fairly complete list is given in reference 1. Some significant works not mentioned in reference 1 are references 2 and 3.

The present report describes a program tailored to the analysis of coupled-cavity traveling-wave tubes on an interactive time-sharing system. Approximations not necessary to keep central-processing-unit (CPU) time within reasonable bounds are avoided. Extreme flexibility is provided in the variety of tube features that can be modeled, since each cavity in the slow-wave structure has individually entered input

parameters. The program can handle lumped or distributed severs, input and output couplers, cavity match details provided for cavities near the end of a stack, voltage-jump velocity resynchronization with an arbitrary number of discrete steps (up to 1 per cavity), and velocity taper designs of almost arbitrary complexity. Backward waves can be handled by an iterative procedure similar to that described in reference 3.

The program was developed to provide an analytical tool for the evaluation of coupled-cavity traveling-wave-tube efficiency enhancement schemes. It also may be used for routine traveling-wave-tube design.

Test cases were constructed for comparison of computed results with the asymptotic Pierce theory. Computed results were also compared with experimental measurements on the 200-watt traveling-wave tube of the Communications Technology Satellite. In both comparisons, agreement was quite good.

MODEL OF COUPLED-CAVITY TRAVELING-WAVE TUBE

Our model of a coupled-cavity traveling-wave tube is illustrated by figure 1. The beam is treated as a series of rigid but mutually penetrable disks. A complete description of the beam trajectory is obtained by following the disks contained in a single beam wavelength (ref. 4). The number of disks per beam wavelength is an adjustable input parameter but is usually set at 24. The diameter of a beam disk ($2r_b$ in fig. 1) is allowed to take on up to three different values during the course of a calculation. This option is provided to accommodate the fact that traveling-wave-tube beams tend to expand in the saturation region of the tube.

Similarly, the charge and mass per disk are allowed to diminish by preselected amounts at two preselected positions within the tube. This allows the program user to roughly estimate the effects on tube gain and efficiency of various amounts of beam interception by the structure.

The tube body is treated as a conducting tunnel (radius a) divided axially into a series of discrete cavities, or cells. In the center of each cavity (length of k^{th} cavity is denoted by L_k) is a gap of length $2l_k$. Impressed across the k^{th} gap is a complex voltage $V_k e^{i\omega t}$. (Symbols are defined in appendix A.)

In the absence of a beam, Floquet's theorem (ref. 5) provides a simple known relationship among the various V_k. For a forward propagating wave in the passband of a uniform structure,

$$V_{k+1} = e^{-(\alpha+i\beta)L} V_k \tag{1}$$

where α and β are known from cold-test measurements. The power flowing along the structure is given by the following equation (from ref. 6):

$$P_k = \frac{|V_k|^2}{2Z_k} \tag{2}$$

where Z_k, the interaction impedance, also is known from cold-test measurements.

The voltage wave in the presence of the beam is calculated by addition of a complex induced voltage to the propagating wave voltage; that is,

$$V_{k+1} = e^{-(\alpha+i\beta)L} V_k + \Delta V_{k+1} \tag{3}$$

where ΔV_{k+1} is an induced voltage to be defined later.

The body of a coupled-cavity traveling-wave tube is supposedly a periodic structure. If this were the case, all cavities would have the same L, ℓ, αL, βL, and Z. However, a real tube has input and output couplers, severs, and perhaps velocity tapers and cavity match details, all of which require individual, nonperiodic treatment in the model. Thus, the properties of individual cavities are separately specified as input parameters in the program so that a great number of tube-design variations such as complicated velocity tapers or voltage-jump configurations can be easily modeled. Equation (3) is easily modified to handle such a quasiperiodic structure by the use of local values of α and β:

$$V_{k+1} = T_{k,k+1} V_k + \Delta V_{k+1} \tag{4}$$

where

$$T_{k,k+1} = \sqrt{\frac{Z_{k+1}}{Z_k}}\, e^{-(\alpha L)_k} e^{-i(\beta L)_k} \tag{5}$$

The factor $\sqrt{Z_{k+1}/Z_k}$ ensures that power flow is conserved.

Floquet's theorem (eq. (1)) strictly applies only to an infinite-length periodic structure. We are actually applying it to a finite-length, almost-periodic structure whose properties may vary slowly with position. Equations (4) and (5) should thus be considered as approximations, analogous to the phase integral method as used in ionospheric radio-wave propagation studies (ref. 7).

MATHEMATICAL FORMULATION

Beam Disk Dynamics

The relativistic energy of a particle can be written as

$$E = \frac{m_0 c^2}{\sqrt{1 - \frac{u_0^2}{c^2}}} + qV_0 \tag{6}$$

Because energy is conserved through the electron gun,

$$\frac{m_0 c^2}{\sqrt{1 - \frac{u_0^2}{c^2}}} = m_0 c^2 + qV_0 \tag{7}$$

which gives directly

$$u_0 = c \sqrt{1 - \frac{1}{\left[1 + \left(\frac{qV_0}{m_0 c^2}\right)\right]^2}} \tag{8}$$

For a V_0 of approximately 10 kilovolts, the relativistic correction is about 1.5 percent. For analysis of a device whose operation depends on near synchronism of the electron beam and the circuit wave, a 1.5-percent error in velocity was thought to be too large to ignore. Thus, relativistic dynamics were used to analyze the beam motion. The velocity change due to an applied force is given by

$$\frac{du_z}{dt} = \frac{F_z}{m_0}\left(1 - \frac{u_z^2}{c^2}\right)^{3/2} \tag{9}$$

Equation (9) is the one-dimensional form of equation (16-58) of reference 8.

Space-charge forces. - In a frame moving along with the beam, the space-charge forces can be determined by the solution to an electrostatics problem. The field of a point charge in a cylindrical tunnel is given by the following equation (from ref. 9):

$$V = \frac{q}{2\pi\epsilon_0 r_a^2} \sum_{\substack{p=1 \\ s=0}}^{\infty} (2 - \delta_{s0}) e^{-\mu_{p,s}|z|} \cos s(\varphi - \varphi_0) \frac{J_s(\mu_{p,s}\rho) J_s(\mu_{p,s}\rho_0)}{\mu_{p,s}\left[J_{s+1}(\mu_{p,s} r_a)\right]^2} \tag{10}$$

where r_a is the beam tunnel radius, and

$$\left.\begin{aligned} J_s(\mu_{p,s} r_a) &= 0 \\ \delta_{s0} &= \begin{cases} 1 & \text{for } s = 0 \\ 0 & \text{for } s \neq 0 \end{cases} \end{aligned}\right\} \tag{11}$$

and the charge is located at $(\rho_0, \varphi_0, 0)$. Consider a beam disk of radius r_b and thickness[1] t_D, centered at ($\rho_0 = 0$; $z_0 = 0$), with uniform charge density σ. With the use of equation (11), it is a straightforward exercise to show that the potential in the tunnel due to the beam disk is given by

$$V_{disk} = \frac{\sigma r_b}{\epsilon_0 r_a^2} \sum_{p=1}^{\infty} \frac{J_0(\mu_{p,0}\rho) J_1(\mu_{p,0} r_b)}{\mu_{p,0}^2 J_1^2(\mu_{p,0} r_a)} \frac{2}{\mu_{p,0}} \begin{cases} e^{-\mu_{p,0}|z|} \sinh \frac{\mu_{p,0} t_D}{2} & \text{for } |z| \geq \frac{t_D}{2} \\ 1 - e^{-\mu_{p,0} t_D/2} \cosh \mu_{p,0} z & \text{for } |z| \leq \frac{t_D}{2} \end{cases} \tag{12}$$

[1] In this analysis, the disk thickness remains an integer submultiple of the initial beam wavelength (u_0/f). A physically more reasonable treatment would allow the disk thickness to vary with its own local velocity. This would, however, add another dimension to the table in which space-charge forces are stored and would substantially increase computing time. We believe the difference in results would be insignificant.

and, further, the mutual repulsion force between two identical disks whose centers are separated by distance z_0 is

$$F_{z,SC} = \frac{4q^2 \operatorname{sgn} z_0}{\pi \epsilon_0 t_D^2 r_b^2 r_a^2} \sum_{p=1}^{\infty} \frac{J_1^2(\mu_{p,0} r_b)}{\mu_{p,0}^4 J_1^2(\mu_{p,0} r_a)}$$

$$\times \begin{cases} 2 \sinh^2 \dfrac{\mu_{p,0} t_D}{2} e^{-\mu_{p,0}|z_0|} & \text{for } |z_0| \geq t_D \\ 1 - e^{-\mu_{p,0} z_0} - e^{-\mu_{p,0} t_D} \sinh \mu_{p,0} z_0 & \text{for } |z_0| \leq t_D \end{cases} \tag{13}$$

where q is the total charge of a disk and is given by

$$q = \pi r_b^2 t_D \sigma \tag{14}$$

and $\operatorname{sgn} z_0$ is the sign of z_0. The axial force is unchanged by a Lorentz transformation. However, axial lengths in equations (10) to (13) should be those in the moving frame. Thus, equation (13) can be used to calculate the space-charge forces directly in the laboratory frame with the following length correction:

$$\begin{Bmatrix} z_0 \\ t_D \end{Bmatrix} \longrightarrow \frac{1}{\sqrt{1 - \dfrac{u_0^2}{c^2}}} \cdot \begin{Bmatrix} z_0 \\ t_D \end{Bmatrix} \tag{15}$$

This analysis assumes that the velocity spread of the particles is small (nonrelativistic). The accuracy would, therefore, deteriorate near the output of a relativistic, very high efficiency tube.

Radio-frequency electric-field forces. - If the complex voltage on a given gap is known, the electric field in the neighboring region can be written in an expansion of the form (from ref. 10)

$$E_z(r,z,t) = \frac{-mV}{2\sinh(ml)} \sum_{n=-\infty}^{\infty} \frac{C_n(m,\beta_n)}{L} \frac{I_0(\gamma_n r)}{I_0(\gamma_n r_a)} e^{i\omega t - i\beta_n z} \tag{16}$$

where

$$C_n(m,\beta_n) = \frac{2l\left[ml \sinh(ml)\cos(\beta_n l) + \beta_n l \cosh(ml)\sin(\beta_n l)\right]}{(ml)^2 + (\beta_n l)^2}$$

$$\beta_n = \beta_0 + \frac{2n\pi}{L}$$

$$\gamma_n = \sqrt{\beta_n^2 - \frac{\omega^2}{c^2}}$$

and $\beta_0 L$ is the lowest order phase shift per cavity. The parameter m is chosen to best suit the geometry of the gap. In the case of very blunt beam tunnel tips, a zero value for m is appropriate, and equation (16) reduces to

$$E_z = \frac{-V}{L} \sum_{n=-\infty}^{\infty} \frac{\sin(\beta_n l)}{\beta_n l} \frac{I_0(\gamma_n r)}{I_0(\gamma_n r_a)} e^{-i\beta_n z + i\omega t} \tag{17}$$

The expansion of equations (16) and (17) is appropriate to a forward-traveling circuit wave. An arbitrary combination of forward- and backward-traveling waves can be represented by

$$E_z = \sum_{n=-\infty}^{\infty} E_n(r)\left(V_F e^{-i\beta_n z} + V_B e^{i\beta_n z}\right) e^{i\omega t} \tag{18}$$

where V_F and V_B are the complex amplitudes of the forward and backward voltage wave, respectively. For convenience, we have defined

$$E_n(r) = \frac{-mC_n(m,\beta_n)}{2L\,\sinh(ml)} \frac{I_0(\gamma_n r)}{I_0(\gamma_n r_a)} \tag{19}$$

Consider a beam disk of radius r_b, thickness t_D, and charge q, and centered at $(r = 0;\ z = z_0)$. A straightforward calculation shows that the force on the disk due to the radio-frequency (RF) electric field is given by

$$F_{z,\,RF} = \frac{qm}{L\,\sinh(ml)} \sum_{n=-\infty}^{\infty} \frac{C_n(m,\beta_n) I_1(\gamma_n r_b)}{\gamma_n r_b I_0(\gamma_n r_a)} \frac{\sin\frac{\beta_n t_D}{2}}{\beta_n \frac{t_D}{2}} \mathrm{Re}\left[\left(V_F e^{-i\beta_n z_0} + V_B e^{i\beta_n z_0}\right) e^{i\omega t}\right] \tag{20}$$

For use in the program, many of the parameters in equation (20) take on a subscript k, since they may vary from one cavity to another. Thus,

$$F_{z,k,\,RF} = \frac{qm}{L_k\,\sinh(ml_k)} \sum_{n=-\infty}^{\infty} \frac{C_{n,k}(m,\beta_{n,k}) I_1(\gamma_{n,k} r_b)}{\gamma_{n,k} r_b I_0(\gamma_{n,k} r_a)} \frac{\sin\frac{\beta_{n,k} t_D}{2}}{\beta_{n,k} \frac{t_D}{2}}$$

$$\times\ \mathrm{Re}\left[\left(V_{F,k} e^{-i\beta_{n,k} z_k} + V_{B,k} e^{i\beta_n z_k}\right) e^{i\omega t}\right] \tag{21}$$

where z_k is measured from the center of the k^{th} gap, and t_D is the disk thickness in the laboratory frame.

Voltage-jump electric-field forces. - If a dc voltage V_J is imposed across a gap in the slow-wave structure, the resultant electric field can be analyzed in a manner similar to the analysis of the radio-frequency electric field discussed earlier. We first note that the axial electric field is an even function of z. We also note that the geometry of the problem typically satisfies the criteria $L >> r_a$, and $L >> l$. Hence, the fields near the gap have decayed to a fairly low level by $z = \pm(L/2)$. We may therefore expect that little error will be introduced if we expand the dc gap field in a Fourier sine

series over the finite interval $-(L/2) < z < (L/2)$. The potential function which satisfies LaPlace's equation and the boundary condition at $\pm(L/2)$ and has the required behavior at $r = 0$ is

$$\varphi = A_0 + B_0 z + \sum_{n=1}^{\infty} B_n \sin(k_n z) I_0(k_n r) \tag{22}$$

with

$$k_n = \frac{2n\pi}{L} \tag{23}$$

For our purposes, A_0 is arbitrary, and since

$$\varphi\left(\frac{L}{2}\right) - \varphi\left(-\frac{L}{2}\right) = V_J$$

we have

$$\varphi = \frac{V_J z}{L} + \sum_{n=1}^{\infty} B_n \sin(k_n z) I_0(k_n r) \tag{24}$$

and

$$E_z = -\frac{V_J}{L} - \sum_{n=1}^{\infty} B_n k_n \cos(k_n z) I_0(k_n r) \tag{25}$$

The coefficients B_n are available to fit the assumed field shape in the gap which we take to be of the form

$$\left.\begin{aligned} E_z(r = r_a) &= -\frac{V_J}{L} - \sum_{n=1}^{\infty} B_n k_n \cos(k_n z) I_0(k_n r_a) \\ &= \begin{cases} E_0 \cosh mz & \text{if } |z| \le l \\ 0 & \text{if } |z| > l \end{cases} \end{aligned}\right\} \tag{26}$$

where

$$E_0 = \frac{mV_J}{2\sinh(m\ell)} \tag{27}$$

The boundary condition at $r = r_a$ leads in the usual way to

$$B_n k_n = \frac{mV_J C_n(m, k_n)}{L \sinh(m\ell) I_0(k_n r_a)} \tag{28}$$

with

$$C_n(m, k_n) = 2\,\frac{m \sinh(m\ell)\cos(k_n\ell) + k_n \cosh(m\ell)\sin(k_n\ell)}{m^2 + k_n^2} \tag{29}$$

Thus, equation (25) becomes

$$E_z = -\frac{V_J}{L} - \frac{mV_J}{L \sinh(m\ell)} \sum_{n=1}^{\infty} \frac{C_n(m, k_n)\cos(k_n z) I_0(k_n r)}{I_0(k_n r_a)} \tag{30}$$

A straightforward analysis shows that the force exerted by this field on a beam disk is given by

$$F_z = \begin{cases} -\dfrac{qV_J}{L}\left[1 + \dfrac{2m}{\sinh(m\ell)} \displaystyle\sum_{n=1}^{\infty} \frac{C_n(m, k_n) I_1(k_n r_b)\cos(k_n z_0)\sin\frac{k_n t_D}{2}}{(k_n r_b) I_0(k_n r_a)\frac{k_n t_D}{2}}\right] & \text{if } |z_0| \le \dfrac{L - t_D}{2} \\ -\dfrac{qV_J}{L}\left\{\dfrac{L + t_D - 2|z_0|}{2t_D} + \dfrac{m}{\sinh(m\ell)} \displaystyle\sum_{n=1}^{\infty} \frac{C_n(m, k_n) I_1(k_n r_b)}{k_n r_b I_0(k_n r_a)}\left[\frac{\sin k_n\left(\frac{t_D}{2} - |z_0|\right)}{\frac{k_n t_D}{2}}\right]\right\} & \text{if } \dfrac{L - t_D}{2} \le |z_0| \le \dfrac{L + t_D}{2} \end{cases} \tag{31}$$

Obviously, F_z equals zero if $|z_0| > (L + t_D)/2$.

Beam-Wave Coupling Analysis

Let $\vec{E}_1$, $\vec{H}_1$ and $\vec{E}_2$, $\vec{H}_2$ be solutions to Maxwell's equations for current sources $\vec{J}_1$ and $\vec{J}_2$, respectively. It is easily shown that

$$\int_S \left[\left(\vec{E}_1^* \times \vec{H}_2\right) + \left(\vec{E}_2 \times \vec{H}_1^*\right)\right] \cdot \vec{n}\, dS = - \int_v \left[\left(\vec{E}_1^* \cdot \vec{J}_2\right) + \left(\vec{E}_2 \cdot \vec{J}_1^*\right)\right] dv \qquad (32)$$

where $\vec{n}$ is an outward-directed unit normal, and S is a closed surface bounding the volume v, and asterisk denotes complex conjugate. We shall use equation (32) to derive an expression for the fields radiated by a current source in a coupled-cavity slow-wave structure. Let v denote a section (volume) of a slow-wave structure bounded by the outer, cylindrical, conducting wall S_0 and any two planes S_B and S_F normal to the axis (see fig. 2). It is immediately clear that the integration over S_0 makes no contribution to the left side of equation (32), since the tangential electric field must vanish on a conducting surface. Thus, equation (32) can be written as

$$\int_{S_F} \left[\left(\vec{E}_1^* \times \vec{H}_2\right) + \left(\vec{E}_2 \times \vec{H}_1^*\right)\right] \cdot \vec{a}_z\, dS - \int_{S_B} \left[\left(\vec{E}_1^* \times \vec{H}_2\right) + \left(\vec{E}_2 \times \vec{H}_1^*\right)\right] \cdot \vec{a}_z\, dS$$

$$= - \int_v \left[\left(\vec{E}_1^* \cdot \vec{J}_2\right) + \left(\vec{E}_2 \cdot \vec{J}_1^*\right)\right] dv \qquad (33)$$

Orthogonality relation for periodic structures. - In equation (33), let $\vec{E}_1$, $\vec{H}_1$ be a backward-propagating wave $\vec{E}_{0,B}$, $\vec{H}_{0,B}$ whose source is outside the volume of interest. Let $\vec{E}_2$, $\vec{H}_2$ be a forward-propagating wave $\vec{E}_{0,F}$, $\vec{H}_{0,F}$ whose source is also outside the volume of interest. The volume integral for this case is zero, and equation (33) can be written as

$$\int_{S_F} \left[\left(\vec{E}_{0,B}^* \times \vec{H}_{0,F}\right) + \left(\vec{E}_{0,F} \times \vec{H}_{0,B}^*\right)\right] \cdot \vec{a}_z\, dS = \int_{S_B} \left[\left(\vec{E}_{0,B}^* \times \vec{H}_{0,F}\right)\right.$$

$$\left. + \left(\vec{E}_{0,F} \times \vec{H}_{0,B}^*\right)\right] \cdot \vec{a}_z\, dS = K \qquad (34)$$

where K is some constant independent of the axial position at which the surface integral is taken.

To determine the value of K, consider the special case in which S_B and S_F are separated by exactly one periodic length. Since the region is source free, the fields must obey Floquet's theorem and hence

$$\begin{Bmatrix} E_{0,F} \\ H_{0,F} \end{Bmatrix}_{S_F} = e^{-i\beta L} \begin{Bmatrix} E_{0,F} \\ H_{0,F} \end{Bmatrix}_{S_B} \tag{35}$$

and

$$\begin{Bmatrix} E_{0,B} \\ H_{0,B} \end{Bmatrix}_{S_F} = e^{i\beta L} \begin{Bmatrix} E_{0,B} \\ H_{0,B} \end{Bmatrix}_{S_B} \tag{36}$$

Thus,

$$\int_{S_F} \left[\left(\vec{E}^*_{0,B} \times \vec{H}_{0,F} \right) + \left(\vec{E}_{0,F} \times \vec{H}^*_{0,B} \right) \right] \cdot \vec{a}_z \, dS = e^{-2i\beta L} \int_{S_B} \left[\left(\vec{E}^*_{0,B} \times \vec{H}_{0,F} \right) + \left(\vec{E}_{0,F} \times \vec{H}^*_{0,B} \right) \right] \cdot \vec{a}_z \, dS \tag{37}$$

Excepting the trivial case where βL is a multiple of π, equations (37) and (34) require that $K = 0$.

Fields radiated by a current source in a slow-wave structure. - Let a source $J_a = J_1(z)e^{i\omega t}$ be present in a single cavity of a periodic coupled-cavity chain. The surfaces S_B and S_F are the axial boundaries of the cavity v ($z = \pm L/2$). Let $\vec{E}_{0,B}$, $\vec{H}_{0,B}$ be the fields of a backward wave whose source is outside the cavity v and whose amplitude is chosen to represent unit power flow. Similarly, let $\vec{E}_{0,F}$, $\vec{H}_{0,F}$ be a unit-amplitude source-free forward wave. Outside the cavity v, the fields radiated by J_a within v are given by

$$\begin{Bmatrix} \vec{E}_a \\ \vec{H}_a \end{Bmatrix} = \begin{Bmatrix} a_F \vec{E}_{0,F} \\ a_F \vec{H}_{0,F} \end{Bmatrix} \quad \text{if } z \geq \frac{L}{2} \tag{38}$$

$$\begin{Bmatrix} \vec{E}_a \\ \vec{H}_a \end{Bmatrix} = \begin{Bmatrix} a_B \vec{E}_{0,B} \\ a_B \vec{H}_{0,B} \end{Bmatrix} \quad \text{if } z \le -\frac{L}{2} \tag{39}$$

where a_F and a_B are complex constants to be determined.

In equation (32), let $\vec{E}_1$, $\vec{H}_1$ be replaced by $\vec{E}_{0,B}$, $\vec{H}_{0,B}$, and let $\vec{E}_2$, $\vec{H}_2$, $\vec{J}_2$ be replaced by $\vec{E}_a$, $\vec{H}_a$, $\vec{J}_a$. The result is

$$a_B \int_{S_B} \left[\left(\vec{E}^*_{0,B} \times \vec{H}_{0,B} \right) + \left(\vec{E}_{0,B} \times \vec{H}^*_{0,B} \right) \right] \cdot \vec{a}_z \, dS - a_F \int_{S_F} \left[\left(\vec{E}^*_{0,B} \times \vec{H}_{0,F} \right) + \left(\vec{E}_{0,F} \times \vec{H}^*_{0,B} \right) \right] \cdot \vec{a}_z \, dS = - \int_v \vec{E}^*_{0,B} \cdot \vec{J}_a \, dv \tag{40}$$

The integral over S_B equals 4, because $\vec{E}_{0,B}$, $\vec{H}_{0,B}$ have been normalized to unit power flow. The integral over S_F equals 0 by virtue of equation (34). Hence,

$$a_B = -\frac{1}{4} \int_v \vec{E}^*_{0,B} \cdot \vec{J}_a \, dv \tag{41}$$

A similar analysis with $\vec{E}_1$, $\vec{H}_1$ in equation (32) replaced by $\vec{E}_{0,F}$, $\vec{H}_{0,F}$ leads to

$$a_F = -\frac{1}{4} \int_v \vec{E}^*_{0,F} \cdot \vec{J}_a \, dv \tag{42}$$

The fields $\vec{E}_{0,B}$, $\vec{E}_{0,F}$ are expressed in the form given by equation (18). The gap voltages $V_{0,F}$ and $V_{0,B}$ must satisfy $(|V|^2/2Z) = 1$, since we have specified unity power flow in the source-free fields. For convenience, we specify zero phase for $V_{0,F}$ and $V_{0,B}$, so that

$$V_{0,F} = V_{0,B} = \sqrt{2Z} \tag{43}$$

and, therefore,

$$a_B = \frac{-\sqrt{2Z}}{4} \int_v \sum_n E_n(r) e^{-i\beta_n z} J_1 dv \tag{44}$$

and

$$a_F = \frac{-\sqrt{2Z}}{4} \int_v \sum_n E_n(r) e^{i\beta_n z} J_1 dv \tag{45}$$

Representation of radiated fields by induced voltage. - Equations (38), (39), (41), and (42) describe the fields radiated by J_a outside the cavity that contains J_a. The result may conveniently be represented by an induced gap voltage ΔV_F which propagates in the forward direction and another, ΔV_B, which propagates in the backward direction. With phase referred to the gap of the cavity containing J_a, the induced voltages are given by

$$\Delta V_F = -\frac{Z}{2} \int_v \sum_n E_n(r) e^{i\beta_n z} J_1(z) dv \tag{46}$$

and

$$\Delta V_B = -\frac{Z}{2} \int_v \sum_n E_n(r) e^{-i\beta_n z} J_1(z) dv \tag{47}$$

Equations (41) and (42) can be used to calculate the effect of J_a on the circuit wave everywhere except within the cavity that contains J_a. These results are not valid within the cavity, because equations (38) and (39) do not apply there. To obtain a result valid within the cavity, consider figure 3, which depicts the power balance within the cavity. The power, P_a, added by J_a is, evidently,

$$P_a = \frac{1}{2Z}\left[2\mathcal{R}e\left(V_F^*\Delta V_F + V_B^*\Delta V_B\right) + |\Delta V_F|^2 + |\Delta V_B|^2\right]$$

$$= \frac{1}{Z}\,\mathcal{R}e\left[\left(V_F + \frac{\Delta V_F}{2}\right)^* \Delta V_F + \left(V_B + \frac{\Delta V_B}{2}\right)^* \Delta V_B\right] \tag{48}$$

Or, with the use of equations (46) and (47),

$$P_a = -\frac{1}{2}\,\mathcal{R}e \int_{\mathcal{v}} \sum_n E_n(r) J_a(z) \left[\left(V_F + \frac{\Delta V_F}{2}\right)^* e^{i\beta_n z} + \left(V_B + \frac{\Delta V_B}{2}\right)^* e^{-i\beta_n z}\right] d\mathcal{v} \tag{49}$$

But, we also know that P_a is given by

$$P_a = -\frac{1}{2}\,\mathcal{R}e \int_{\mathcal{v}} \vec{E}^* \cdot \vec{J}_a \, d\mathcal{v} \tag{50}$$

Hence, correct results will be obtained if the forward- and backward-propagating gap voltages which act upon the beam within the cavity are set equal to $\left[V_F + (\Delta V_F/2)\right]$ and $\left[V_B + (\Delta V_B/2)\right]$, respectively. In the preceding analysis, V_F and V_B are the gap voltages due to fields which propagate in from neighboring cavities and are independent of J_a; the induced voltages ΔV_F and ΔV_B are given by equations (46) and (47).

Power-Balance Verification

Consider the section of a traveling-wave tube beginning at the input end of the tube and terminating at the exit plane of the k^{th} cavity. At the input end, power enters in the form of beam kinetic energy ($I_0 V_0$) and input radio-frequency drive (P_0) and leaves in the form of backward wave power ($P_{B,1}$) propagating back into the driving source. At the output end of the test section under consideration, power enters in the form of backward-wave power ($P_{B,k+1}$) propagating back from cavity k+1 and leaves in the form of beam kinetic power ($P_{b,k}$) and forward-wave radio-frequency power ($P_{F,k}$). If

there are any voltage-jump cavities within the test section, they add power

$$\sum_{j=1}^{k} P_{J,j}$$

Finally, power is dissipated by joule heating within the test section

$$\sum_{j=1}^{k} P_{LOSS,j}$$

A test parameter can be defined by writing the power balance within the test section. In the notation defined above,

$$I_0V_0 + P_0 - P_{B,1} + P_{B,k+1} - P_{b,k} - P_{F,k} + \sum_{j=1}^{k} P_{J,j} = \sum_{j=1}^{k} P_{LOSS,j} \tag{51}$$

or

$$\alpha_{PB,k} = \frac{P_{b,k} + P_{F,k} + P_{B,1} + \sum_{j=1}^{k} P_{LOSS,j} - \sum_{j=1}^{k} P_{J,j} - P_0 - P_{B,k+1}}{I_0V_0} \tag{52}$$

The parameter $\alpha_{PB,k}$ is calculated for every cavity and printed out as an independent check on other calculations; obviously, it should equal unity. Individual contributions to this parameter are

$$P_{b,k} = \frac{\omega}{2\pi} \sum_{i=1}^{N_d} m_D c^2 \left[\frac{1}{\sqrt{1 - \frac{u_i^2}{c^2}}} - 1 \right] \tag{53}$$

where m_D is the rest mass of a beam disk, u_i is the axial velocity of the i^{th} disk at the exit plane of the k^{th} cavity, and the sum is over the disks in an entering beam wavelength. Also,

$$P_{b,0} = I_0 V_0 \tag{54}$$

$$P_{F,k} = \frac{|V_{F,k}|^2}{2Z_k} \tag{55}$$

$$P_{B,k} = \frac{|V_{B,k}|^2}{2Z_k} \tag{56}$$

$$P_{J,j} = I_0 V_{J,j} \tag{57}$$

$$P_{LOSS,j} = (P_{F,j} + P_{B,j}) \left[1 - e^{-2(\alpha L)_j}\right] \tag{58}$$

Equation (58) is correct only if the forward and backward waves are 90^o out of phase and thus not coupled by cavity wall losses. However, the errors due to use of equation (58) will tend to average out to zero when a large number of cavities with a variety of phase angles are included in the test section. Usually, $P_{F,j} >> P_{B,j}$, which further diminishes the importance of this error. Finally, the joule-heating loss is usually not one of the largest terms in equation (51). Therefore, equation (58) seems to be a fairly safe approximation.

A more important error is neglect of space-charge potential energy transported by the beam. For high perveance devices, this may equal a significant fraction of the beam kinetic power (ref. 11). However, the magnitude and direction of the error can be estimated. In the case of low perveance devices ($\approx 0.1 \times 10^{-6}$ $AV^{-3/2}$), it is negligible. And the energy balance parameter serves only as a running check on the other calculations. Because accounting for beam potential energy would significantly increase computer time, this was not done.

PROGRAM STRUCTURE

Input Data

The inputs required by the program, the units in which the inputs are entered into the program, and the symbol used for each input are as follows:

Beam voltage, V . . . . . V_0

Beam current, mA . . . . . I_0

Input power, dBm . . . . . P_0

Frequency, GHz . . . . . f

Beam tunnel radius, cm . . . . . r_a

I^{th} beam radius, cm . . . . . $r_{b,i}$

Electric field shaping parameter . . . . . m

Number of beam radii . . . . . N_b

Number of cavities . . . . . N_c

Number of disks per beam wavelength . . . . . N_d

Number of nodes per cavity . . . . . N_z

For the k^{th} cavity:

Cavity periodic length, cm . . . . . L_k

Gap length, cm . . . . . $2\ell_k$

Propagation loss across cavity in forward direction, dB . . . . . $(\alpha L)_{F,k}$

Propagation loss across cavity in backward direction, dB . . . . . $(\alpha L)_{B,k}$

Interaction impedance, ohms . . . . . Z_k

Phase shift parameter . . . . . $\left[(\beta_1 L)/\pi\right]_k$

dc voltage jump, V . . . . . $V_{J,k}$

Beam Disk Dynamics

The computational problem discussed in this section is how to calculate beam disk trajectories in a suitable manner. Ordinarily, the computational procedure is to solve for the disk acceleration, as given by equation (9). Numerical integration of this equa-

tion then yields $u_i(t)$, the velocity of the i^{th} disk at time t. Numerical integration of $u_i(t)$ yields $z_i(t)$, the axial position of the i^{th} disk at time t. Instead of using the functions $u_i(t)$ and $z_i(t)$ to describe the trajectories, it is more convenient for our purposes to let z be the independent variable and to calculate the functions $dt_i(z)/dz$ and $t_i(z)$. Here, $dt_i(z)/dz$ is the reciprocal of the velocity of the i^{th} disk when it reaches the axial position z, and $t_i(z)$ is the time of arrival of the i^{th} disk at the axial position z. In terms of these new functions, the equations of motion are

$$\frac{d^2t_i}{dz^2} = -\frac{F_{z,i}}{m_D}\left[1 - \frac{1}{\left(\frac{dt_i}{dz}\cdot c\right)^2}\right]^{3/2}\left(\frac{dt_i}{dz}\right)^3 \quad \text{for } i = 1, 2, \ldots, N_d \tag{59}$$

where $F_{z,i}$ is the total axial force on the i^{th} disk.

The coordinate system used in the program has its origin at the beginning of the first cavity. The k^{th} cavity is divided into N_z equal parts of length Δz_k given by

$$\Delta z_k = \frac{L_k}{N_z} \tag{60}$$

The n^{th} node in the first cavity, denoted by $z_{n,1}$, is defined by

$$z_{n,1} = n\,\Delta z_1 \quad \text{for } n = 0, 1, \ldots, N_z \tag{61}$$

The n^{th} node in the k^{th} cavity, denoted by $z_{n,k}$, is defined by

$$z_{n,k} = \sum_{m=1}^{k-1} L_m + n\,\Delta z_k \quad \text{for} \begin{cases} n = 0, 1, \ldots, N_z \\ k = 2, 3, \ldots, N_c \end{cases} \tag{62}$$

A point which lies midway between two nodes $z_{n,k}$ and $z_{n+1,k}$ is denoted by $z_{n+\frac{1}{2},k}$. Such a point will be called the n^{th} antinode in cavity k. The numerical integration of equation (59) is such that the functions d^2t_i/dz^2 are evaluated at nodes, and the functions dt_i/dz and $t_i(z)$ are evaluated at antinodes.

At some point in cavity k, we have trajectory data at node $n-1$ and antinode $n-1$;

that is, the functions $d^2t_i(z_{n-1,k})/dz^2$, $dt_i(z_{n-\frac{1}{2},k})/dz$, and $t_i(z_{n-\frac{1}{2},k})$ are known. The problem now is to obtain $d^2t_i(z_{n,k})/dz^2$, $dt_i(z_{n+\frac{1}{2},k})/dz$, and $t_i(z_{n+\frac{1}{2},k})$. We first obtain approximations for $dt_i(z_{n,k})/dz$ and $t_i(z_{n,k})$ with the equations

$$\frac{dt_i(z_{n,k})}{dz} = \frac{dt_i(z_{n-\frac{1}{2},k})}{dz} + \frac{d^2t_i(z_{n-1,k})}{dz^2} \cdot \frac{\Delta z_k}{2} \tag{63}$$

$$t_i(z_{n,k}) = t_i(z_{n-\frac{1}{2},k}) + \frac{dt_i(z_{n-\frac{1}{2},k})}{dz} \cdot \frac{\Delta z_k}{2} + \frac{1}{2} \frac{d^2t_i(z_{n-1,k})}{dz^2} \left(\frac{\Delta z_k}{2}\right)^2 \tag{64}$$

Knowing, at least approximately, $dt_i(z_{n,k})/dz$ and $t_i(z_{n,k})$, we can evaluate $d^2t_i(z_{n,k})/dz^2$ from equation (59). We now obtain $dt_i(z_{n+\frac{1}{2},k})/dz$ and $t_i(z_{n+\frac{1}{2},k})$ by the equations

$$\frac{dt_i(z_{n+\frac{1}{2},k})}{dz} = \frac{dt_i(z_{n-\frac{1}{2},k})}{dz} + \frac{d^2t_i(z_{n,k})}{dz^2} \Delta z_k \tag{65}$$

$$t_i(z_{n+\frac{1}{2},k}) = t_i(z_{n-\frac{1}{2},k}) + \frac{dt_i(z_{n-\frac{1}{2},k})}{dz} \Delta z_k + \frac{d^2t_i(z_{n,k})}{dz^2} \frac{\Delta z_k^2}{2} \tag{66}$$

Space-charge forces. - The space-charge force on one disk due to another with a separation distance of z_0 is given by equation (13). Use of this equation for calculating space-charge forces on each integration step would be intolerably slow. The method used here is to set up N_b tables, where each table contains 50 data points corresponding to 50 separation distances. The n^{th} data point would be the space-charge force between two disks, as calculated by equation (13), separated by the n^{th} separation distance. In the computer simulation, the space-charge force on one disk due to another is calculated by the use of linear interpolation on the appropriate table.

Fortunately, the space-charge force on a given disk is a slowly-varying function of the independent variable z. This is especially true in the beginning cavities of the tube. To take advantage of the slowly-varying nature of the space-charge force, the calculation is not done on every integration step. The calculation of space-charge forces is initially done every M^{th} step, where M is an input. During the simulation,

M may change in a manner to be described later. On those integration steps where space-charge forces are not calculated, they are approximated by quadratic curve-fits. Each disk has its own curve-fit. These curve-fits are obtained by fitting a quadratic polynomial through the latest three calculations of space-charge forces. Let us say that these three calculations were done when z was equal to z_a, z_b, and z_c. At an integration step where a new space-charge force calculation is due, at $z = z_d$, the values calculated are compared with those obtained when the curve-fits based on the points z_a, z_b, and z_c are evaluated at z_d. If the difference in the values for any disk is exceeded by a specified tolerance, the next calculation of space-charge forces occurs $\frac{1}{2}M$ steps later. In general, M is halved each time the specified tolerance is exceeded.

For calculating space-charge forces, the positions of all disks must be known at a time t. This information is not readily available, since z rather than t is the independent variable. To calculate the space-charge force on the i^{th} disk located at some z, we must determine the positions of all the other disks at the time $t_i(z)$. Consider the j^{th} disk. The time of arrival, $t_j(z)$, at z is known. By the periodicity of the motion, the disk which originally was m wavelengths behind the j^{th} disk arrives at z at the time $t_j(z) + mT$. Similarly, the disk which originally was m wavelengths ahead of the j^{th} disk arrives at z at the time $t_j(z) + (-m)T$. We consider all such disks and find m such that

$$\left| t_i(z) - \left[t_j(z) + mT \right] \right| = \text{minimum} \tag{67}$$

We may call the disk in question the j^{th} disk in the m^{th} cycle. We assume that the j^{th} disk in any other cycle is too far away from the i^{th} disk at the time $t_i(z)$ to make a significant contribution to the space-charge force on the i^{th} disk. Let z_j be the position of the j^{th} disk in the m^{th} cycle at the time $t_i(z)$. We obtain z_j by assuming this disk has constant velocity $u_j(z)$ in the time interval spanned by $t_i(z)$ and $t_j(z) + mT$. Then z_j is given by

$$z_j = z + u_j(z) \left\{ t_i(z) - \left[t_j(z) + mT \right] \right\} \tag{68}$$

The space-charge force is then calculated on the basis of the separation distance $z - z_j$. The calculation is done for all disks, excluding the i^{th} disk, and the results are summed to obtain the total space-charge force on the i^{th} disk. When the separation distance $z - z_j$ is greater than a specified number, the space-charge calculation is not done for this term in the summation.

Radio-frequency electric-field forces. - The radio-frequency electric-field force

on a disk is given by equation (21). The z_k in this equation is the axial position relative to the center of the k^{th} cavity. In the present notation, z_k will be replaced by $y_{n,k}$. Thus, $y_{n,k}$ is the axial position of the n^{th} node in the k^{th} cavity relative to the center of the cavity. In equation form, $y_{n,k}$ is related to $z_{n,k}$ by

$$y_{n,k} = z_{n,k} - \left(\sum_{m=1}^{k-1} L_m + \frac{L_k}{2} \right) \tag{69}$$

We define $Q_{n,k}$ by

$$Q_{n,k} = \frac{q\mu}{L_k \ell_k \sinh(\mu)} \sum_{m=-\infty}^{\infty} \frac{C_{m,k}(\mu, \beta_{m,k}) I_1(\gamma_{m,k} r_{b,k})}{\gamma_{m,k} r_{b,k} I_0(\gamma_{m,k} r_a)} \cdot \left(\frac{\sin \frac{\beta_{m,k} t_D}{2}}{\frac{\beta_{m,k} t_D}{2}} \right) e^{-i\beta_{m,k} y_{n,k}}$$

$$\text{for} \begin{cases} n = 0, 1, \ldots, N_z \\ k = 1, 2, \ldots, N_c \end{cases} \tag{70}$$

where $\mu = m\ell_k$. Then, the electric field force on the i^{th} disk located at $z_{n,k}$ is given by

$$F_{i,n,k} = Re\left[\left(Q_{n,k} V_{F,k} + Q^*_{n,k} V_{B,k} \right) e^{i\omega t_i (z_{n,k})} \right] \tag{71}$$

The $Q_{n,k}$ are calculated and stored in a table when cavity k is entered. The number of terms of the summation used to calculate each table entry is an adjustable input parameter. If cavity k has the same L_k, ℓ_k, $\beta_{0,k}$ as cavity k-1, then $Q_{n,k-1} = Q_{n,k}$, and a new table does not have to be calculated. When a new table does have to be calculated, the old table is no longer needed, and the new table may occupy the same storage space as the old table had occupied. The electric-field force is evaluated by equation (71).

Voltage-jump electric-field forces. - The voltage-jump electric-field force on a disk is given by equation (31). The technique for evaluating voltage-jump electric-field forces is essentially the same as for evaluating radio-frequency electric-field forces. We define $R_{n,k}$ by the equations

$$R_{n,k} = \frac{-q}{L_k}\left[1 + \frac{2\mu}{\ell_k \sinh(\mu)} \sum_{m=1}^{\infty} \frac{C_m(\mu, k_m) I_1(k_m r_{b,k}) \sin\left(\frac{k_m t_D}{2}\right) \cos(k_m y_{n,k})}{k_m r_{b,k} I_0(k_m r_a)\left(\frac{k_m t_D}{2}\right)}\right]$$

$$\text{if } |y_{n,k}| \le \frac{L_k - t_D}{2} \qquad (72a)$$

$$R_{n,k} = \frac{-q}{L_k}\left[\frac{L_k + t_D - 2|y_{n,k}|}{2t_D} + \frac{\mu}{\ell_k \sinh(\mu)} \sum_{m=1}^{\infty} \frac{C_m(\mu, k_m) I_1(k_m r_{b,k}) \sin\left(\frac{k_m t_D}{2} - k_m |y_{n,k}|\right)}{k_m r_{b,k} I_0(k_m r_a)\left(\frac{k_m t_D}{2}\right)}\right]$$

$$\text{if } \frac{L_k - t_D}{2} \le |y_{n,k}| \le \frac{L_k + t_D}{2} \qquad (72b)$$

Let $V_{J,k}$ be the voltage jump associated with cavity k. Then, the electric-field force on a disk located at $z_{n,k}$ is given by

$$F_{n,k} = R_{n,k} V_{J,k} \qquad (73)$$

The $R_{n,k}$ are calculated and stored in a table and have the same features as the $Q_{n,k}$ for radio-frequency electric-field forces.

Beam-Wave Coupling Analysis

The parameters of interest in the beam-wave interaction are the induced voltages, ΔV_F and ΔV_B. These are obtained from equations (46) and (47). We proceed to use these equations to develop expressions for ΔV_F and ΔV_B which are computationally convenient. The appropriate Fourier component of the beam current, $J_1(z)$, is given by

$$J_1(z) = \frac{1}{T}\int_{t-T}^{t} J_z(z, t')e^{-i\omega t'}\, dt' \tag{74}$$

We define $P_{m,k}$ by

$$P_{m,k} = \pi \frac{\mu r_{b,k} C_{m,k}(\mu, \beta_{m,k}) Z_k I_1(\gamma_{m,k} r_{b,k})}{\ell_k L_k \sinh(\mu)\gamma_{m,k} I_0(\gamma_{m,k} r_a)} \tag{75}$$

With the use of equations (19), (46), and (47), we obtain for cavity k

$$\Delta V_{F,k} = \int_{-L_k/2}^{L_k/2} \sum_{m=-\infty}^{\infty} P_{m,k} e^{i\beta_{m,k} z} J_1(z)dz \tag{76}$$

$$\Delta V_{B,k} = \int_{-L_k/2}^{L_k/2} \sum_{m=-\infty}^{\infty} P_{m,k} e^{-i\beta_{m,k} z} J_1(z)dz \tag{77}$$

In equations (76) and (77), the integration variable z is the axial position relative to the center of cavity k. The integrals in equations (76) and (77) are evaluated with the use of Simpson's rule. Thus,

$$\Delta V_{F,k} = \Delta z_k \sum_{n=0}^{N_z} \delta_n \sum_{m=-\infty}^{\infty} P_{m,k} e^{i\beta_{m,k} y_{n,k}} J_1(z_{n,k}) \tag{78}$$

$$\Delta V_{B,k} = \Delta z_k \sum_{n=0}^{N_z} \delta_n \sum_{m=-\infty}^{\infty} P_{m,k} e^{-i\beta_{m,k} y_{n,k}} J_1(z_{n,k}) \tag{79}$$

where

$$\delta_n = \begin{cases} \frac{1}{3} & \text{if } n = 0 \text{ or } n = N_z \\ \frac{2}{3} & \text{if } n \neq 0,\ n \neq N_z, \text{ and } n \text{ is an odd integer} \\ \frac{4}{3} & \text{if } n \neq 0,\ n \neq N_z, \text{ and } n \text{ is an even integer} \end{cases}$$

We define $S_{n,k}$ by

$$S_{n,k} = \sum_{m=-\infty}^{\infty} P_{m,k} e^{i\beta_{m,k} y_{n,k}} \tag{80}$$

The $S_{n,k}$ values are calculated and stored in a table that has the same features as the $Q_{n,k}$ and $R_{n,k}$ tables. Appendix B gives a derivation of the following expression for $J_1(z_{n,k})$:

$$J_1(z_{n,k}) = \frac{q}{\pi r_b^2 T} \sum_{i=1}^{N_d} \frac{\sin\left[\frac{\omega t_D}{2u_i(z_{n,k})}\right]}{\left[\frac{\omega t_D}{2u_i(z_{n,k})}\right]} e^{-i\omega t_i(z_{n,k})} \tag{81}$$

Our final expressions for $\Delta V_{F,k}$ and $\Delta V_{B,k}$ are

$$\Delta V_{F,k} = \Delta z_k \sum_{n=0}^{N_z} \delta_n S_{n,k} J_1(z_{n,k}) \tag{82}$$

$$\Delta V_{B,K} = \Delta z_k \sum_{n=0}^{N_z} \delta_n S^*_{n,k} J_1(z_{n,k}) \tag{83}$$

Calculating the effects of the backward wave requires an iterative procedure. In the first pass through the tube, the $\Delta V_{B,k}$ values are calculated and stored for each cavity k. From the values of $\Delta V_{B,k}$, the backward voltages for a cavity chain from cavity k1 to cavity k2 are obtained from equations (4) and (5) and the results of the Beam-Wave Coupling Analysis section.

$$V_{B,k2} = \frac{1}{2} \Delta V_{B,k2} \tag{84}$$

$$V_{B,k} = \frac{\Delta V_{B,k}}{2} + \left(V_{B,k+1} + \frac{\Delta V_{B,k+1}}{2} \right) \sqrt{\frac{Z_k}{Z_{k+1}}}\, e^{-(\alpha L)_{B,k}} e^{-i(\beta_1 L)_k}$$

$$\text{for } k = (k2 - 1), (k2 - 2), \ldots, k1 \tag{85}$$

With the known values of $V_{B,k}$ for the desired cavities, a second pass is made through the tube. The second pass yields a new set of $\Delta V_{B,k}$ values, which can be used for calculating a set of $V_{B,k}$ values for a third pass. The process continues until convergence is obtained. In many applications, the iterative procedure will converge faster if the iteration is done on one tube section at a time. This would be true, for example, for a tube having severs. The program has the capability of performing the iterative procedure for an arbitrary set of cavity chains.

The computational procedure in the beam-wave interaction process is as follows:

(1) When cavity k is entered, the summation $S_{n,k}$ in equation (80) is calculated and stored for each node n. If cavity k has the same L_k, l_k, $\beta_{0,k}$, and $r_{b,k}$ as has cavity k-1, then $S_{n,k} = S_{n,k-1}$, and a new table does not have to be calculated.

(2) A first approximation to $\Delta V_{F,k}$ is obtained by assuming the disks have constant velocity in cavity k. Thus,

$$t_i(z_{n,k}) = t_i(z_{0,k}) + \frac{dt_i(z_{0,k})}{dz}\,(z_{n,k} - z_{0,k}) \tag{86}$$

With $t_i(z_{n,k})$ known, $J_1(z_{n,k})$ can be calculated from equation (81), and then $\Delta V_{F,k}$ can be calculated from equation (82).

(3) Let the forward voltage for cavity k be

$$V_{F,k} = \sqrt{\frac{Z_k}{Z_{k-1}}}\left[\left(V_{F,k-1} + \frac{1}{2}\Delta V_{F,k-1}\right) e^{-(\alpha L)_{F,k-1}}\, e^{-i(\beta_1 L)_{k-1}}\right] + \frac{1}{2}\Delta V_{F,k} \tag{87}$$

If there is a backward voltage, it is assumed to be known from use of equation (85) with the set of $\Delta V_{B,k}$ obtained from the previous pass through the tube.

(4) Numerical integration of the equations of motion is used to obtain $t_i(z_{n,k})$ for $n = 1$ to $n = N_z$.

(5) At the n^{th} node in the cavity, after $t_i(z_{n,k})$ has been obtained, $\delta_n S_{n,k} J_1(z_{n,k})$ and $\delta_n S^*_{n,k} J_1(z_{n,k})$ are calculated and stored. These quantities are the n^{th} terms in the summations of equations (82) and (83).

(6) When the last integration step in cavity k has been done, a better approximation of $\Delta V_{F,k}$ is calculated from equation (82). The $\Delta V_{F,k}$ so obtained replaces the old $\Delta V_{F,k}$ calculated in step 2. Also, $\Delta V_{B,k}$ is calculated from equation (83). The $\Delta V_{B,k}$ values are stored for use in the next pass through the tube.

(7) If additional accuracy is required, steps 3 to 6 are repeated.

(8) Steps 1 to 7 are repeated for cavity k+1.

(9) When the last cavity is done, and the effects of the backward wave are to be determined, a second pass is made through the tube. The backward voltages for the second pass are determined from the $\Delta V_{B,k}$ values of the first pass.

(10) As many passes are made through the tube as are required to obtain convergence.

Power-Balance Verification

The equations for power balance, equations (52) to (58), are in a form that can be implemented without any modifications. It is worth noting that one of the advantages of using z rather than t as the independent variable is in calculating the kinetic power, $P_{k,k}$. From equation (53), $P_{b,k}$ is easily calculated, since the values of $u_i(z)$ are

known. If t were the independent variable, one would have to keep track of each disk as it passed the point z in question and calculate $u_i(z)$ by an interpolation procedure.

Summary of Program Steps

The entire computational procedure may be summarized by the following steps:

(1) Input data are read.

(2) The tables for space-charge forces are calculated.

(3) Numerical integration of equations of motion is begun with z as the independent variable. At each step, the radio-frequency forces and, if required, the voltage-jump forces are calculated. The space-charge forces are calculated either by quadratic curve fits or by linear interpolations on the appropriate tables.

(4) At the end of each step, it is determined whether data are to be stored for plotting.

(5) When a new cavity is entered, let us say the k^{th} cavity, the data for cavity $k-1$ are printed out. If the parameters of cavity k are different from those of cavity $k-1$, the tables which are required for evaluation of radio-frequency forces, voltage-jump forces, and induced voltages are calculated. A first approximation of $\Delta V_{F,k}$ is obtained by assuming the disks have constant velocity throughout cavity k. The forward voltage for cavity k is obtained by attenuating and phase-shifting $V_{F,k-1}$ and adding the result vectorially to $\Delta V_{F,k}/2$.

(6) When the last integration step in cavity k has been done, a better approximation of $\Delta V_{F,k}$ is calculated. Also, $\Delta V_{B,k}$ is calculated.

(7) If additional accuracy is required, a second pass is made through cavity k.

(8) For cavity $k+1$, steps 5 to 7 are repeated.

(9) If the effects of the backward wave are to be determined, a second pass is made through the tube.

(10) As many passes are made through the tube as are required to obtain convergence.

RESULTS AND DISCUSSION

The coupled-cavity program has been tested by appropriate comparison with the asymptotic Pierce theory (ref. 12) and also with experimental results obtained on the 200-watt traveling-wave tube of the Communications Technology Satellite (refs. 13 to 15).

Comparison of Analytical Results With Asymptotic Pierce Theory

In program runs to be compared with the asymptotic Pierce theory, the relativistic corrections and all space harmonics other than the first forward one were suppressed. The backward wave is, of course, ignored in both calculations. Program inputs describing circuit and beam parameters were chosen to achieve predetermined values of Pierce's C and QC over a range of values of b. Input power and tube length were chosen so that, for each value of C and QC, gain exceeded 20 decibels over most or all of the range of b, and tube output remained well below saturation. In all runs, the step-size parameters were chosen as 24 disks per beam wavelength, and 16 axial mesh points per period. The space-charge calculation was cut off at a disk separation distance of $6.5\lambda_B/24$.

In each case, tube gain, calculated as above, was compared with values given by the asymptotic Pierce theory (i.e., from ref. 12).

$$G = A + BCN \tag{88}$$

$$A = 20 \log \left\{ \left| \frac{\delta_1^2}{(\delta_1 - \delta_2)(\delta_1 - \delta_3)} \right| \cdot \left| \frac{\delta_1^2 + 4\,QC}{\delta_1^2} \right| \right\} \tag{89}$$

$$C = \left(\frac{K_1 I_0}{4V_0} \right)^{1/3} \tag{90}$$

$$N = \frac{\omega L_T}{2\pi u_0} \tag{91}$$

$$B = 54.6 \cdot Re\,(\delta_1) \tag{92}$$

$$QC = \frac{R\omega_p^2}{\omega^2 + R\omega_p^2} \tag{93}$$

The space-charge reduction parameter R was obtained from figure 9.3-3 of reference 12 which was stored as a table.

At first, the propagation constants δ_1, δ_2, and δ_3 were obtained by calculating the roots of the cubic determinantal equation appropriate to the small C approximation (ref. 12).

$$\delta^2 = \frac{1}{(-b + id + i\delta)} - 4QC \tag{94}$$

However, at moderate values of $|Cb|$ (i.e., when $|Cb| \gtrsim 0.1$), rather large discrepancies appeared between the results of the asymptotic Pierce theory and the coupled-cavity program. The discrepancies did not significantly diminish when the number of disks per beam wavelength or mesh points per period was increased. It appeared, therefore, that the fault might be in the approximations leading to equation (94). A more exact fourth-order determinantal equation was then obtained from equation (10.1-35) in reference 12.

$$\delta^2 = \frac{(1 + Cb - iCd)(1 + Cb)^2}{(-b + i\delta + id) - \frac{C}{2}\left[\delta^2 - (b - id)^2\right]} - 4QC \tag{95}$$

It is clear that equation (95) reduces to equation (94) if one assumes $C \ll 1$. However, the error in δ^2 will be of order $(1 + Cb)^3 - 1 \approx 3Cb$. Subsequent calculations of asymptotic Pierce gain used the three roots of equation (95) corresponding to forward waves. Roots of equation (95) were found by a simple iterative procedure that used a root of equation (94) as a first approximation.

After this refinement, agreement between the coupled-cavity program and the Pierce asymptotic theory was found to be satisfactory. The comparison for a range of parameters is shown in figure 4.

Comparison of Analytical Results With Measured Data

Tube design. - The design of the 200-watt traveling-wave tube for the Communications Technology Satellite (CTS) was determined largely by others, prior to the development of our large-signal program. Subsequently, because of project schedule restrictions, only a few minor design changes which addressed major defects were allowed. The most important of these changes are described in reference 15.

The design beam voltage, beam current, nominal beam diameter, and tunnel diameter are 11.1 kilovolts, 70 milliamperes, 0.635 millimeter, and 1.27 millimeters,

respectively. The standard cavities in the gain sections of the tube have a periodic length of 3.175 millimeters and a gap length of 0.965 millimeter.

The slow-wave structure has a rather large cold bandwidth of about 1300 megahertz, with the 85-megahertz CTS band centered near a phase shift per cavity of 1.2 π in all sections of the tube.

The number and types of cavities in the CTS tube are shown in figure 5. The three gain sections are separated by severs. The three velocity-taper sections are separated by transition regions in which the phase velocity (or periodic length) changes gradually from one cavity to the next. Each sever consists of two modified cavities, each containing tuning stubs and silicon carbide - beryllium oxide loads. Forward and backward circuit waves are completely terminated at a sever, since there is no coupling slot in the wall between the two sever cavities. Two additional cavities adjacent to the input and output couplers and on each side of the two severs are modified for match purposes. These cavities have extra long coupling slots and thus extra wide cold bandwidth; they provide a reduced contribution to the gain of the tube and have much different electrical properties than their neighbors.

The beam tunnel tips are rather blunt, so the parameter m in equation (16) was taken as zero.

Raw cold-test data obtained with uniform stacks of 5 to 10 cavities were available for many of the particular cavity geometries including all of those for which there was more than one cavity per tube. Phase velocity and interaction impedance, at the frequencies of interest, were calculated from the cold-test data by use of published methods (refs. 6 and 16). Results were interpolated or, in two cases, extrapolated to cover those 10 cavities for which cold-test data were not available. Accurate insertion loss measurements on brazed tube sections were also available. Values for propagation loss per cavity were obtained by dividing the insertion loss measurements, in a reasonable way, among the cavities within a given section. Resulting input data used for the calculation are given in tables I to IV.

Comparison of results. - Computed results and corresponding experimental data for the CTS traveling-wave tube are presented in figures 6 to 8. All measurements were obtained with a beam voltage of 11.3 kilovolts and beam current of 71 milliamperes. Beam current interception was typically 1 milliampere under small-signal conditions and 4.5 milliamperes at saturation conditions. Calculations were also made with a beam voltage of 11.3 kilovolts, but the beam current was taken as 70 milliamperes in order to make an approximate allowance for current and power removed from the beam by interception. The beam diameter used in the calculation was the nominal value of 0.635 millimeter (one-half the tunnel diameter). Results are shown for the first iteration with backward wave ignored, and for the final result after several iterations with the backward wave included in the calculation. Three iterations were usually

sufficient to converge to the point where further change was negligible.

Figure 6 shows small-signal gain as a function of frequency. Ignoring the gain ripple, which is assumed to be due to internal reflections, the agreement between measurement and calculation is excellent. The first iteration, without considering the backward wave, is also in good agreement with experiment. However, a significant discrepancy begins to appear near the lower edge of the band. In this particular tube, the π point was around 11.925 gigahertz.

Figure 7 shows saturation drive as a function of frequency. Again, agreement between calculation and experiment is excellent. The first iteration again shows appreciable errors only near the lower edge of the frequency band.

Figure 8 shows saturation output power as a function of frequency. Agreement between calculation and experiment is within about 0.5 decibel (about 3 percent of input beam power), with the calculated power usually being somewhat higher than the measured power. This is comparable to the amount of additional power dissipated by beam interception under saturation conditions which also varied somewhat with frequency. The effect of ignoring the backward wave was a further increase of 0.5 to 1 decibel in computed output power. This discrepancy was observed everywhere in the passband and became a bit larger near the lower edge of the band.

Limited calculations were also made with other values of nominal beam diameter. A 10-percent increase in beam diameter produced about a 1-decibel increase in gain and a 0.1-decibel increase in output power; a like decrease in beam diameter had the opposite effect. No appreciable change was observed in the shapes of the various curves as beam diameter was varied. In all of these calculations, the internal check on power balance was satisfied extremely well, with the discrepancy rarely exceeding 0.1 percent and never exceeding 0.2 percent. Computer central processing unit (CPU) time required for a single iteration was less than 1.5 seconds per cavity.

CONCLUDING REMARKS

A flexible, accurate, large-signal computer program has been developed for analysis of coupled-cavity traveling-wave tubes. The program was written in FORTRAN IV for an IBM 360/67 time-sharing system. The central processing unit (CPU) time for a single pass through the tube is about 1.5 seconds per cavity. The beam is described by a disk model, and the slow-wave structure by a sequence of cavities, or cells. The computational approach is arranged so that each cavity may have geometrical or electrical parameters different from those of its neighbors. This allows the program user to simulate a tube of almost arbitrary complexity. Input and output couplers, severs, complicated velocity tapers, and other features peculiar to one or a few cavities may be

modeled by a correct choice of input parameters. The beam-wave interaction is handled by a new approach in which the radio-frequency fields are expanded in solutions to the transverse magnetic wave equation retaining all significant space harmonics. The program was used to perform a design study of the traveling-wave tube developed for the Communications Technology Satellite (CTS). The computed results were in good agreement with the measured data from the flight tube. The agreement for saturation drive and small-signal gain was within 1 or 2 decibels, and saturation output power agreed within about 3 percent of input beam power. The internal check on power balance was satisfied within 0.2 percent.

The small-signal gain calculated by the program was also compared with the asymptotic Pierce theory over a broad range of beam and circuit parameters. A modified form of the asymptotic Pierce theory, which did not include the assumption that Pierce's gain parameter was very small, was used. Agreement in this comparison was also quite good.

Lewis Research Center,
National Aeronautics and Space Administration,
Cleveland, Ohio, March 18, 1977,
506-20.

APPENDIX A

SYMBOLS

A	Pierce launching-loss parameter, defined in eq. (89)
A_0	constant of integration in eq. (22)
a_B	complex amplitude coefficient for induced backward wave
a_F	complex amplitude coefficient for induced forward wave
$\vec{a}_z$	unit vector in the z direction
B	Pierce gain parameter, defined in eq. (92)
B_n	constant of integration in eq. (22)
B_0	constant of integration in eq. (22)
b	Pierce velocity parameter, defined in ref. 12
C	Pierce interaction parameter, defined in eq. (90)
$C_n(m, k_n)$	parameter defined in eq. (29)
$C_n(m, \beta_n)$	parameter defined after eq. (16)
c	velocity of light in free space
d	Pierce loss parameter, defined in ref. 12
E	energy
E_a	electric field due to current source J_a
$E_n(r)$	amplitude parameter defined in eq. (19)
E_z	axial component of electric field
$\vec{E}$	electric field
$\vec{E}_{0,B}$	backward-propagating, source-free electric field
$\vec{E}_{0,F}$	forward-propagating, source-free electric field
$F_{i,n,k}$	force parameter defined in eq. (71)
$F_{n,k}$	force parameter defined in eq. (73)
F_z	total axial force
$F_{z,i}$	total axial force on i^{th} disk
$F_{z,k}$	axial component of force associated with k^{th} cavity
$F_{z,RF}$	axial force on a beam disk due to radio-frequency fields

$F_{z, SC}$	repulsive space-charge force between two beam disks
f	frequency (program input parameter)
G	gain (see eq. (88))
H_a	magnetic field due to current source J_a
$\vec{H}$	magnetic-field strength
$\vec{H}_{0, B}$	magnetic-field strength associated with source-free backward wave
$\vec{H}_{0, F}$	magnetic-field strength associated with source-free forward wave
I_0	beam current (program input parameter)
$I_s(x)$	modified Bessel function of order s and argument x
i	$\sqrt{-1}$
J(z, t)	current density
J_a	current source
$J_s(x)$	Bessel function of order s and argument x
J_z	axial component of current
$J_1(z)$	Fourier component of the beam current density
$\vec{J}$	current
j	summation index
K	result of surface integration, defined in eq. (34)
K_1	Pierce interaction impedance, defined in ref. 12
k_n	eigenvalue defined by eq. (23)
L	periodic length of a cavity
L_k	periodic length of k^{th} cavity (program input parameter)
L_T	length of tube
ℓ	half of gap length
ℓ_k	half of gap length of k^{th} cavity (program input parameter)
m	electric-field shape parameter used in eq. (16) (program input parameter)
m_D	rest mass of a beam disk
m_0	rest mass of a particle
N	length of a tube in units of beam wavelength
N_b	number of beam radii (program input parameter)

N_c	number of cavities (program input parameter)
N_d	number of disks per beam wavelength (program input parameter)
N_z	number of nodes per cavity (program input parameter)
n	summation index
$\vec{n}$	a unit vector normal to a surface
P_a	power added to wave by current source J_a
$P_{B,k}$	backward wave power at k^{th} cavity
$P_{b,k}$	beam kinetic power at k^{th} cavity
$P_{F,k}$	forward wave power at k^{th} cavity
$P_{J,k}$	voltage-jump power at k^{th} cavity
P_k	power at k^{th} cavity
$P_{LOSS,k}$	propagation loss at k^{th} cavity
P_0	radio-frequency input power (program input parameter)
p	summation index
QC	Pierce space-charge parameter, defined by eq. (93)
q	charge of a beam disk
R	space-charge reduction factor, defined in ref. 12
r	radius
r_a	beam tunnel radius
r_b	beam radius
$r_{b,i}$	i^{th} beam radius (program input parameter)
$r_{b,k}$	beam radius in k^{th} cavity
S	a surface
S_B	back surface of a section of a slow-wave structure (see fig. 2)
S_F	front surface of a section of a slow-wave structure (see fig. 2)
S_0	outer, cylindrical, conducting surface of a section of a slow-wave structure (see fig. 2)
s	summation index
T	period of a radio-frequency cycle (1/f)
$T_{k,k+1}$	transformation defined by eq. (5)

t	time
t_D	thickness of a beam disk
$t_i^m(z)$	arrival time of i^{th} disk in m^{th} radio-frequency cycle at axial position z
u	velocity
u_i	velocity of i^{th} disk
u_z	axial component of velocity
u_0	initial beam velocity
V	voltage or potential
$V_{B,k}$	backward voltage on k^{th} gap
$\Delta V_{B,k}$	backward voltage on k^{th} gap induced by the beam current in k^{th} cavity
$V_{F,k}$	forward voltage on k^{th} gap
$\Delta V_{F,k}$	forward voltage on k^{th} gap induced by the beam current in k^{th} cavity
V_J	voltage-jump voltage
$V_{J,k}$	voltage-jump voltage on k^{th} gap
V_k	voltage on k^{th} gap
ΔV_k	voltage on k^{th} gap induced by the beam current in k^{th} cavity
V_0	beam voltage (program input parameter)
$V_{0,B}$	gap voltage associated with source-free backward wave
$V_{0,F}$	gap voltage associated with source-free forward wave
v	volume
$\mathrm{sgn}(x)$	sign of x (positive if $x \geq 0$; negative if $x < 0$)
$y_{n,k}$	measure of axial position defined in eq. (69)
Z	interaction impedance
Z_k	interaction impedance of k^{th} cavity (program input parameter)
z	axial position
$\mathcal{R}e(z)$	real part of a complex parameter z
$z_i(t)$	axial position of i^{th} disk at time t
z_k	axial position referred to center of k^{th} cavity

Δz_k	length of integration interval for k^{th} cavity
$z_{n,k}$	position of n^{th} node in k^{th} cavity
$z_{n+\frac{1}{2},k}$	position of n^{th} antinode in k^{th} cavity
z_0	axial separation of two beam disks
α	propagation loss per unit length
$\alpha_{PB,k}$	power-balance parameter defined by eq. (52)
$(\alpha L)_{B,k}$	propagation loss across k^{th} cavity in backward direction (program input parameter)
$(\alpha L)_{F,k}$	propagation loss across k^{th} cavity in forward direction (program input parameter)
$(\alpha L)_k$	propagation loss across k^{th} cavity
β	phase shift per unit length (axial wave number)
β_n	phase shift per unit length of n^{th} space harmonic
$(\beta L)_k$	phase shift across k^{th} cavity
$(\beta_1 L/\pi)_k$	parameter proportional to phase shift across k^{th} cavity (program input parameter)
γ_n	radial wave number of n^{th} space harmonic
δ	solution of eq. (94) or (95)
δ_{s0}	parameter defined by eq. (11)
$\delta_1, \delta_2, \delta_3$	Pierce propagation constants (see eq. (89))
ϵ_0	permittivity of free space
λ_B	beam wavelength
μ	normalized electric-field shape parameter
$\mu_{p,s}$	parameter defined by eq. (11) $\left(\mu_{p,s} r_a \text{ is the } p^{th} \text{ zero of } J_s(x)\right)$
ρ, ρ_0	radial coordinates
σ	charge density
φ, φ_0	azimuthal coordinates
ω	angular frequency ($2\pi f$)
ω_p	beam plasma frequency (see ref. 12)

APPENDIX B

DERIVATION OF FOURIER COMPONENT OF BEAM CURRENT DENSITY

In the section on program structure, $J_1(z)$ was defined (eq. (74)) as

$$J_1(z) = \frac{1}{T} \int_{t-T}^{t} J(z, t') e^{-i\omega t'} \, dt' \tag{B1}$$

We proceed to obtain an expression for $J_1(z)$ which is convenient for computation. Let $t_i^m(z)$ be the time of arrival at z of the i^{th} disk in the m^{th} radio-frequency cycle. We let $m = 0$ for the radio-frequency cycle considered in the program. To conform with previous notation, we will henceforth omit the 0 superscript when referring to the cycle considered in the program; that is, $t_i^0(z) \equiv t_i(z)$. Then, for any integer m,

$$t_i^m(z) = t_i(z) - mT \tag{B2}$$

Consider $J(z, t)$ as a function of t for some fixed z (see fig. 9). At $t = t_i^m(z)$, the value of $J(z, t)$ is $\sigma u_i(z)$, where σ is the charge density of a disk. Furthermore, $J(z, t)$ has this value for a time interval centered about $t_i^m(z)$, where the length of the interval is $t_D/u_i(z)$. We can express this partial contribution to $J(z, t)$ by using the unit step function U in the following way:

$$\sigma u_i(z) \left(U\left\{ \left[t - t_i^m(z) \right] + \frac{t_D}{2u_i(z)} \right\} - U\left\{ \left[t - t_i^m(z) \right] - \frac{t_D}{2u_i(z)} \right\} \right)$$

For more concise notation, we define the function h as

$$h\left\{ \left[t - t_i^m(z) \right], \frac{t_D}{2u_i(z)} \right\} = U\left\{ \left[t - t_i^m(z) \right] + \frac{t_D}{2u_i(z)} \right\} - U\left\{ \left[t - t_i^m(z) \right] - \frac{t_D}{2u_i(z)} \right\} \tag{B3}$$

The partial contribution to $J(z, t)$ can now be written as

$$\sigma u_i(z) h\left\{ \left[t - t_i^m(z) \right], \frac{t_D}{2u_i(z)} \right\}$$

The total contribution to $J(z, t)$ is obtained by summing over all disks and all cycles.

$$J(z,t) = \sum_{i=1}^{N_d} \sum_{m=-\infty}^{\infty} \sigma u_i(z) h\left\{\left[t - t_i^m(z)\right], \frac{t_D}{2u_i(z)}\right\} \tag{B4}$$

We then have for $J_1(z)$

$$J_1(z) = \frac{1}{T} \sum_{i=1}^{N_d} \sum_{m=-\infty}^{\infty} \sigma u_i(z) \int_{t-T}^{t} e^{-i\omega t'} h\left\{\left[t' - t_i^m(z)\right], \frac{t_D}{2u_i(z)}\right\} dt' \tag{B5}$$

By the periodicity of the motion, there will be N_d disks passing the position z in the time interval from $t-T$ to t. In general, the N_d disks do not all come from the same radio-frequency cycle. Let m_i be the cycle number of the i^{th} disk. From equations (B2) and (B5) we obtain

$$J_1(z) = \frac{1}{T} \sum_{i=1}^{N_d} \sigma u_i(z) \int_{t_{i1}}^{t_{i2}} e^{-i\omega t'} dt' \tag{B6}$$

where t_{i1} and t_{i2} are given by

$$t_{i1} = t_i(z) - m_i T - \frac{t_D}{2u_i(z)} \tag{B7}$$

$$t_{i2} = t_i(z) - m_i T + \frac{t_D}{2u_i(z)} \tag{B8}$$

Evaluating the integral in equation (B6) yields

$$J_1(z) = \frac{1}{T} \sum_{i=1}^{N_d} \sigma t_D \frac{\sin\left[\frac{\omega t_D}{2u_i(z)}\right]}{\left[\frac{\omega t_D}{2u_i(z)}\right]} e^{-i\omega\left[t_i(z)-m_i T\right]} \tag{B9}$$

Since $\omega m_i T = 2\pi m_i$, we have

$$J_1(z) = \frac{1}{T} \sum_{i=1}^{N_d} \sigma t_D \frac{\sin\left[\frac{\omega t_D}{2u_i(z)}\right]}{\left[\frac{\omega t_D}{2u_i(z)}\right]} e^{-i\omega t_i(z)} \tag{B10}$$

The charge density σ can be expressed as

$$\sigma = \frac{q}{\pi r_b^2 t_D} \tag{B11}$$

Combining equations (B10) and (B11) yields

$$J_1(z) = \frac{1}{T} \frac{q}{\pi r_b^2} \sum_{i=1}^{N_d} \frac{\sin\left[\frac{\omega t_D}{2u_i(z)}\right]}{\left[\frac{\omega t_D}{2u_i(z)}\right]} e^{-i\omega t_i(z)} \tag{B12}$$

REFERENCES

1. Mendel, John T.: Helix and Coupled-Cavity Traveling-Wave Tubes. Proc. IEEE, vol. 61, no. 3, Mar. 1973, pp. 280–298.
2. Vaughan, J. Rodney M.: Calculation of Coupled Cavity TWT Performance. IEEE Trans. Electron Devices, vol. ED-22, no. 10, Oct. 1975, pp. 880–890.
3. Kino, G. S.; et al.: Small-Signal and Large-Signal Theories for the Coupled Cavity TWT. Proc. Sixth Int. Conf. on Microwave and Optical Generation and Amplification. IEE-Publ-27, Inst. Electr. Eng., 1966, pp. 49–53.
4. Tien, P. K.; Walker, L. R.; and Wolontis, V. M.: A Large Signal Theory of Traveling-Wave Amplifiers. Proc. IRE, vol. 43, Mar. 1955, pp. 260–277.
5. Watkins, Dean A.: Topics in Electromagnetic Theory. John Wiley & Sons, 1958, pp. 2–4.
6. Connolly, Denis J.: Determination of the Interaction Impedance of Coupled Cavity Slow Wave Structures. IEEE Trans. Electron Devices, vol. ED-23, no. 5, May 1976, pp. 491–493.
7. Budden, K. G.: Radio Waves in the Ionosphere. Cambridge Univ. Press, 1961.
8. Panofsky, Wolfgang K. H.; and Phillips, Melba: Classical Electricity and Magnetism. Addison-Wesley Publishing Co., 1955.
9. Smythe, William R.: Static and Dynamic Electricity. 3rd ed., McGraw-Hill Book Co., Inc., 1968, p. 188.
10. Kosmahl, Henry G.; and Branch, Gorland M.: Generalized Representation of Electric Fields in Interaction Gaps of Klystrons and Traveling-Wave Tubes. IEEE Trans. Electron Devices, vol. ED-20, no. 7, July 1973, pp. 621–629.
11. Hechtel, J. Richard: The Effect of Potential Beam Energy on the Performance of Linear Beam Devices. IEEE Trans. Electron Devices, vol. ED-17, no. 11, Nov. 1970, pp. 999–1009.
12. Gewartowski, James W.; and Watson, H. A.: Principles of Electron Tubes, Including Grid-Controlled Tubes, Microwave Tubes, and Gas Tubes. Van Nostrand, 1965.
13. Franklin, C. A.; and Davison, E. H.: A High Power Communications Technology Satellite for the 12 and 14 GHz Bands. AIAA Paper 72-580, April 1972.
14. Kosmahl, Henry G.; McNary, B. D.; and Sauseng, Otto: High-Efficiency 200-Watt, 12-Gigahertz Traveling Wave Tube. NASA TN D-7709, 1974.

15. Connolly, Denis J.; Forman, Ralph; Jones, C. L.; Kosmahl, Henry G.; and Sharp, G. Richard: Communications Technology Satellite Output-Tube Design and Development. NASA TM X-3480, 1977.

16. Johnson, Curtis C.: Field and Wave Electrodynamics. McGraw-Hill Book Co., Inc., 1965, pp. 269-270.

TABLE I. - PROPAGATION LOSS PER CAVITY

Cavity	Frequency, f, GHz				
	12.00	12.05	12.10	12.15	12.20
	Propagation loss per cavity $(\alpha L)_k$, dB				
1 and 2	0.1	0.1	0.1	0.1	0.1
3 to 9	.09	.07	.06	.05	.05
10 and 11	.1	.1	.1	.1	.1
[a]12	350.0	350.0	350.0	350.0	350.0
13 and 14	.1	.1	.1	.1	.1
15 to 25	.09	.07	.06	.05	.05
26 and 27	.1	.1	.1	.1	.1
[a]28	350.0	350.0	350.0	350.0	350.0
29 and 30	.1	.1	.1	.1	.1
31 to 39	.09	.07	.06	.05	.05
40 to 43	.095	.075	.065	.055	.055
44 and 45	.1	.08	.07	.06	.06
46	.105	.085	.075	.065	.065
47 to 51	.11	.09	.08	.07	.07
52	.12	.1	.09	.08	.08
53	.13	.11	.1	.19	.09
54 and 55	.14	.12	.11	.1	.1
56 to 58	.1	.1	.1	.1	.1

[a]Sever.

TABLE II. - PHASE SHIFT PER CAVITY

Cavity	Frequency, f, GHz				
	12.00	12.05	12.10	12.15	12.20
	Phase shift per cavity, $(\beta_1 L/\pi)_k$, rad				
1	1.48	1.50	1.51	1.53	1.54
2	1.32	1.34	1.36	1.39	1.41
3 to 9	1.16	1.20	1.23	1.27	1.30
10	1.32	1.34	1.36	1.39	1.41
11 to 13	1.48	1.50	1.51	1.53	1.54
14	1.32	1.34	1.36	1.39	1.41
15 to 25	1.16	1.20	1.23	1.27	1.30
26	1.32	1.34	1.36	1.39	1.41
27 to 29	1.48	1.50	1.51	1.53	1.54
30	1.32	1.34	1.36	1.39	1.41
31 to 39	1.16	1.20	1.23	1.27	1.30
40 to 42	1.16	1.21	1.25	1.29	1.32
43 to 47	1.16	1.20	1.25	1.28	1.31
48 to 56	1.17	1.21	1.24	1.27	1.30
57	1.32	1.34	1.36	1.39	1.41
58	1.48	1.50	1.51	1.53	1.54

TABLE III. - INTERACTION IMPEDANCE

Cavity	Frequency, f, GHz				
	12.00	12.05	12.10	12.15	12.20
	Interaction impedance, Z, ohms				
1	400	400	400	400	400
2	850	800	780	750	730
3	1550	1450	1375	1280	1230
4 to 9	1990	1830	1725	1605	1530
10	1550	1450	1375	1280	1230
11	850	800	780	750	730
12 and 13	400	400	400	400	400
14	850	800	780	750	730
15	1550	1450	1375	1280	1230
16 to 25	1990	1830	1725	1605	1530
26	1550	1450	1375	1280	1230
27	850	800	780	750	730
28 and 29	400	400	400	400	400
30	850	800	780	750	730
31	1550	1450	1375	1280	1230
32 to 39	1990	1830	1725	1605	1530
40 to 42	2390	2015	1795	1630	1535
43	2300	1900	1710	1550	1475
44	2150	1800	1620	1470	1400
45	2000	1700	1530	1390	1330
46	1850	1600	1440	1310	1250
47 to 51	1700	1500	1350	1255	1170
52	1600	1350	1240	1150	1150
53	1400	1200	1130	1050	1060
54 and 55	1295	1115	1015	930	960
56	1000	875	810	750	700
57	550	520	500	475	460
58	300	300	300	300	300

TABLE IV. - CAVITY DIMENSIONS

Cavity	Periodic length, L_k, cm	Gap length, $2l_k$, cm
1 to 39	0.3175	0.0965
40 to 42	.3048	.0914
43	.2985	.0899
44	.2921	.0879
45	.2794	.0843
46	.2667	.0808
47 to 51	.2540	.0772
52	.2413	.0739
53	.2286	.0701
54 to 58	.2159	.0660

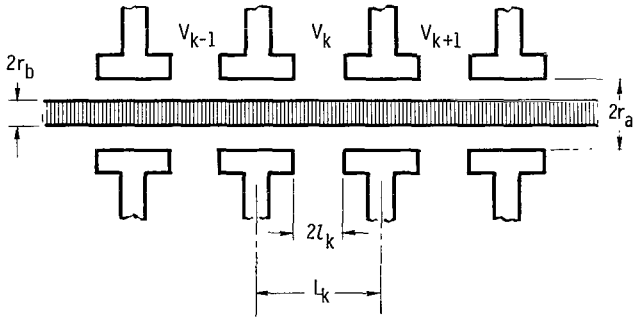

Figure 1. - Geometry of coupled-cavity traveling-wave tube model.

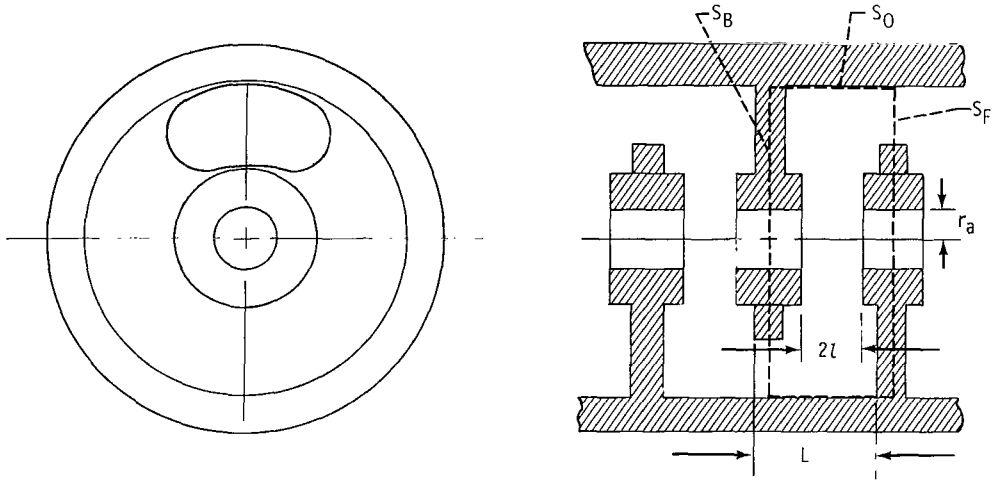

Figure 2. - Geometry of slow-wave structure.

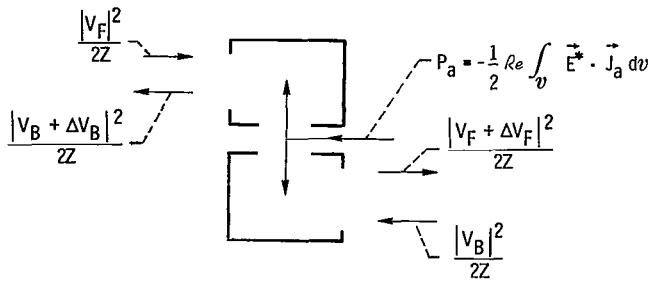

Figure 3. - Power balance in a cavity.

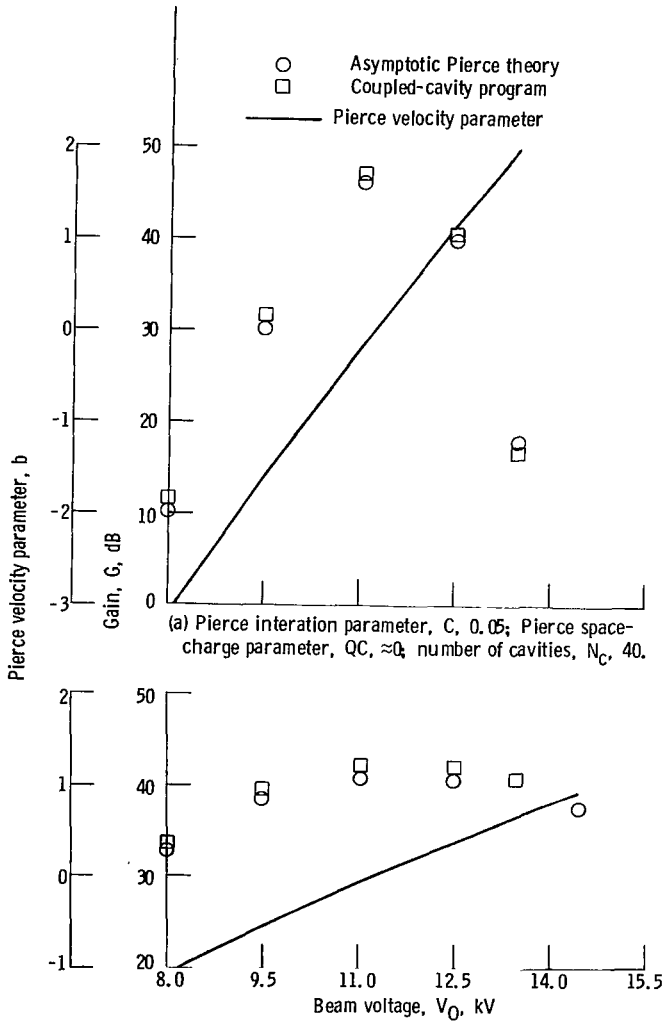

(a) Pierce interation parameter, C, 0.05; Pierce space-charge parameter, QC, ≈0; number of cavities, N_c, 40.

(b) Pierce interaction parameter, C, 0.15; Pierce space-charge parameter, QC, ≈0; number of cavities, N_c, 12.

Figure 4. - Comparison of asymptotic Pierce theory with coupled-cavity program.

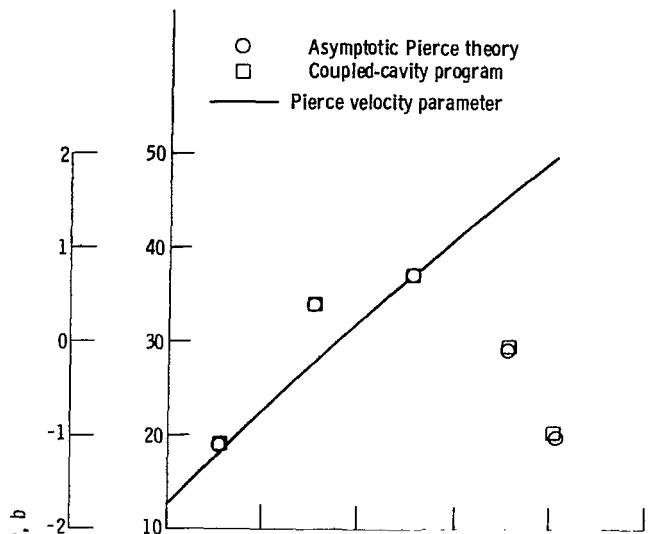

(c) Pierce interaction parameter, C, 0.05; Pierce space-charge parameter, QC, 0.1; number of cavities, N_c, 35.

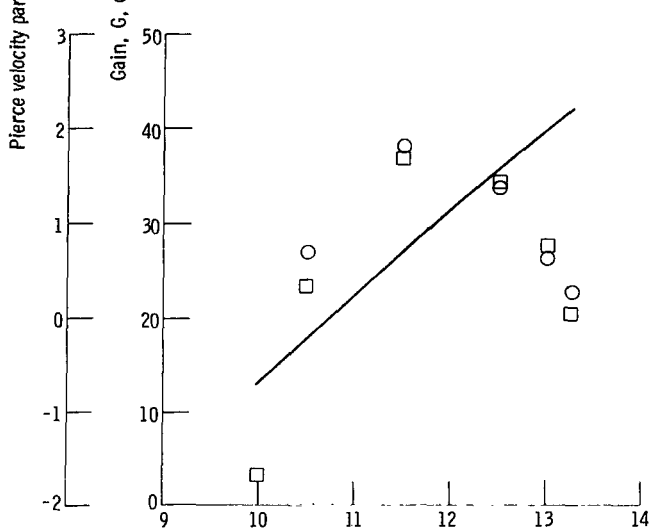

(d) Pierce interaction parameter, C, 0.05; Pierce space-charge parameter, QC, 0.25; number of cavities, N_c, 40.

Figure 4. - Concluded.

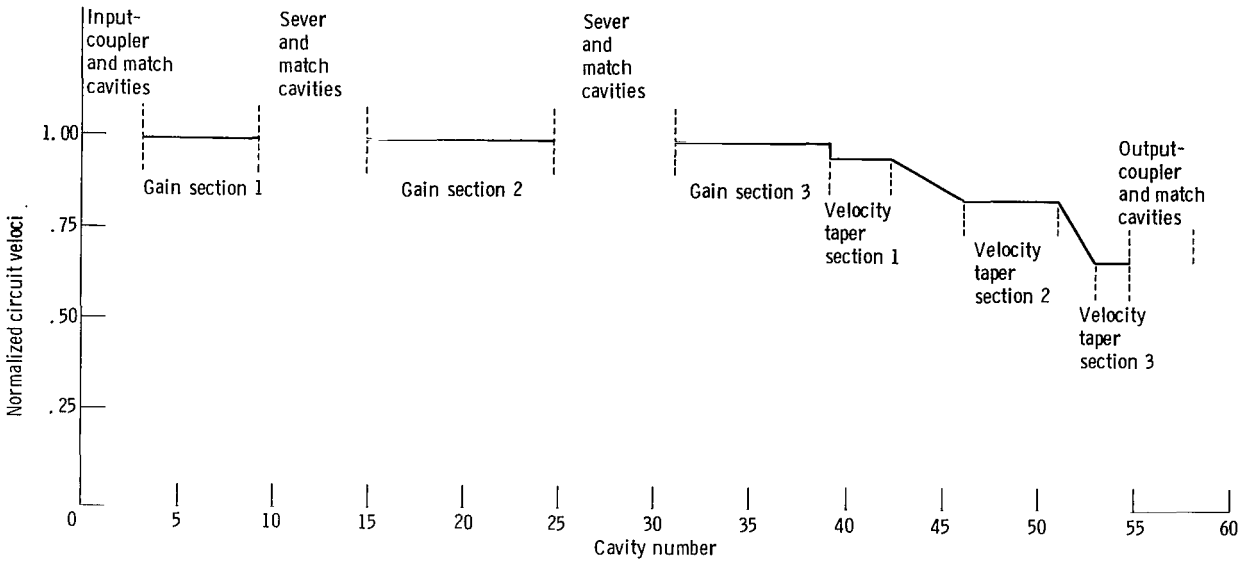

Figure 5. - Normalized circuit velocity as function of cavity number.

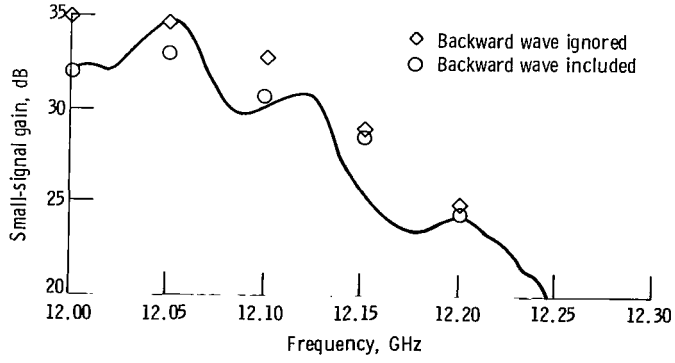

Figure 6. - Small-signal gain versus frequency (0 dBm drive).

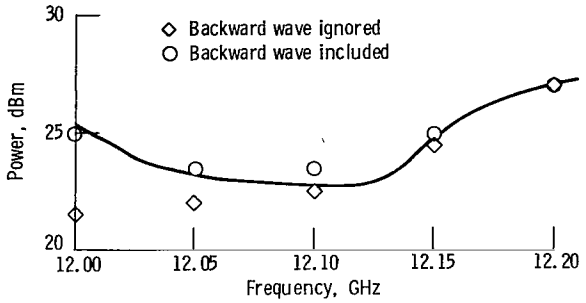

Figure 7. - Input power required to saturate tube versus frequency.

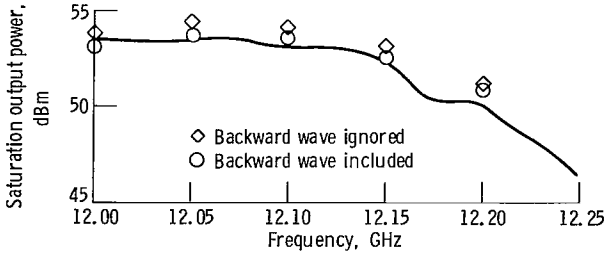

Figure 8. - Saturation output power versus frequency.

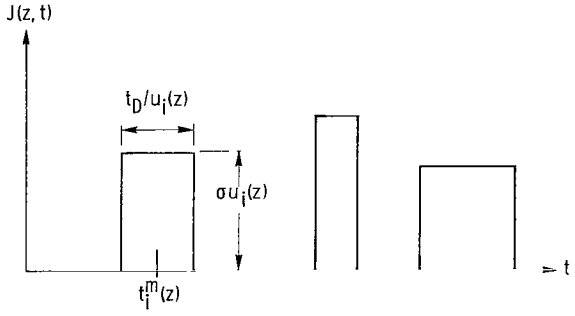

Figure 9. - Current density J(z, t) as a function of t for some fixed z.

"The aeronautical and space activities of the United States shall be conducted so as to contribute . . . to the expansion of human knowledge of phenomena in the atmosphere and space. The Administration shall provide for the widest practicable and appropriate dissemination of information concerning its activities and the results thereof."

—NATIONAL AERONAUTICS AND SPACE ACT OF 1958

NASA SCIENTIFIC AND TECHNICAL PUBLICATIONS

TECHNICAL REPORTS: Scientific and technical information considered important, complete, and a lasting contribution to existing knowledge.

TECHNICAL NOTES: Information less broad in scope but nevertheless of importance as a contribution to existing knowledge.

TECHNICAL MEMORANDUMS: Information receiving limited distribution because of preliminary data, security classification, or other reasons. Also includes conference proceedings with either limited or unlimited distribution.

CONTRACTOR REPORTS: Scientific and technical information generated under a NASA contract or grant and considered an important contribution to existing knowledge.

TECHNICAL TRANSLATIONS: Information published in a foreign language considered to merit NASA distribution in English.

SPECIAL PUBLICATIONS: Information derived from or of value to NASA activities. Publications include final reports of major projects, monographs, data compilations, handbooks, sourcebooks, and special bibliographies.

TECHNOLOGY UTILIZATION PUBLICATIONS: Information on technology used by NASA that may be of particular interest in commercial and other non-aerospace applications. Publications include Tech Briefs, Technology Utilization Reports and Technology Surveys.

Details on the availability of these publications may be obtained from:

SCIENTIFIC AND TECHNICAL INFORMATION OFFICE

NATIONAL AERONAUTICS AND SPACE ADMINISTRATION

Washington, D.C. 20546